Exact solutions for the macro-, meso- and micro-scale analysis of composite laminates and sandwich structures

Exact solutions for the macro-, meso- and micro-scale analysis of composite laminates and sandwich structures

Yang Yan[a,b*], Alfonso Pagani[b†], Erasmo Carrera[b‡], Qingwen Ren[a§]

[a] *College of Mechanics and Materials, Hohai University, 210098, Nanjing, China.*
[b] *Mul^2, Department of Mechanical and Aerospace Engineering, Politecnico di Torino, Corso Duca degli Abruzzi 24, 10129 Torino, Italy*

Submitted to

Journal of Composite Materials

Author for correspondence:
E. Carrera, Professor of Aerospace Structures and Aeroelasticity,
Department of Mechanical and Aerospace Engineering,
Politecnico di Torino,
Corso Duca degli Abruzzi 24,
10129 Torino, Italy,
tel: +39 011 090 6836,
fax: +39 011 090 6899,
e-mail: erasmo.carrera@polito.it

*PhD Student, e-mail: yanyanghhu@hhu.edu.cn
†Assistant Professor, e-mail: alfonso.pagani@polito.it
‡Professor of Aerospace Structures andAeroelasticity, e-mail: erasmo.carrera@polito.it
§Professor of Mechanics and Materials, e-mail: renqw@hhu.edu.cn

ABSTRACT

The present work proposes a closed-form solution based on refined beam theories for the static analysis of fiber-reinforced composite and sandwich beams under simply supported boundary conditions. The higher-order beam models are developed by employing Carrera Unified Formulation (CUF), which uses Lagrange-polynomials expansions (LE) to approximate the kinematic field over the cross section. The CUF-LE allows one to carry out analysis of composite structure analysis through a single formulation in global-local sense, i.e., homogenized laminates at a global scale and fiber-matrix constituents at a local scale, leading to component-wise (CW) analysis. Therefore, three-dimensional (3D) stress/displacement fields at different scales can be successfully detected by increasing the order of Lagrange-polynomials opportunely. The governing equations are derived in a strong-form and solved in a Navier-type sense. Three benchmark numerical assessments are carried out on a single-layer transversely isotropic beam, a cross-ply laminate $[0°/90°/0°]$ *beam and a sandwich beam. The results show that accurate displacement and stress values can be obtained in different parts of the structure with lower computational cost in comparison with CUF finite element method (CUF-FEM) and 3D FEM. Besides, this study may serve as benchmarks for future assessments in this field.*

1 Introduction

Over the last few decades, fiber-reinforced composite materials have been widely employed in many civil and aerospace structures, see for instance the C919 vertical tail manufactured by AVIC Shenyang Aircraft Corporation (SAC, Liaoning, China). A main advantage is that composite materials have better fatigue resistance and corrosion resistance in addition to high strength- and stiffness-to-weight ratios [1] if compared to the traditional metallic materials like steels [2]. These excellent material properties, in turn, result in mass production of corresponding composite components. In spite of this, there are still many key issues to be addressed, e.g., the correct description of progressive damage and failure behavior. Micro-structural effects, e.g., fiber volume fraction, fiber packing and orientation and constituent properties, play a key role in the determination of various modes of failure macroscopically, including fiber tow kinking in compression, tow breakage in tension, and matrix cracking [3]. A better prediction of these complicated failure phenomena resides in the development of an enhanced structured model, which can provide a better prediction of stress/displacement fields of the matrices, fibers, layers and interfaces of the components and unveil the structural failure mechanism further.

The multiscale approach, as a useful tool for composite structures, has received a considerable attention and numerous works have been addressed in the literature. A brief but not exhaustive review is given here. Usually, the precision of the multiscale model depends on the rationality of the micromechanical model, which correlates the properties of matrix-fiber cells with those of composite laminates. A common evaluation of the effective elastic behavior of unidirectional fiber-reinforced composite laminates is the analytical models, providing a explicit formulation in terms of the geometry, position and properties of constituents under simple loading conditions [4]. Some of well-known models can be found in the literature: the rule of mixture [5, 6, 7] , the Mori-Tanaka method [8, 9], the Hashin-Shtrikman bounds [10] and the generalized self-consistent method [11]. Although analytical models are easy to implement, they cannot detect the local stress and strain fields in the fiber-matrix constituent. To this purpose, other semi-analytical and numerical methods have been put forward sequentially to retrieve more accurate local fields. Examples are the Generalised Method of Cells (GMC) [12, 13], the Representative Volume Element (RVE) [14, 15], the variational asymptotic method for unit cell homogenization (VAMUCH) [16] and the Mechanics of Structure Genome (MSG) [17, 18, 19]. Recently, an elaborate description of bottom-up, multiscale modelling approach for high-fidelity virtual mechanical tests of composite materials has been presented in [20], which used molecular dynamics and Monte Carlo methods at nano-scale, RVEs at micro-scale and structural elements (beams, plates or shells) at macro-scale.

To some extent, the most critical issues in a multiscale simulation are the trade-off between computational efforts and the high-fidelity analysis, which may affect its reliability and application into the real engineering structures. Therefore, a proper research on this issue is in sustained growth, aiming at providing an

approximate solution with an acceptable error and simultaneous increasing efficiency [21].

In the present work, a novel approach referred to Component-Wise (CW) is introduced to carry out the global-local analysis of heterogeneous structures at multiple scales based on a variable kinematic 1D model and rule of mixture. CW means that components of different scales can be modelled at the same time. In this sense, users can tune the model according to the practical demands to use micro-scale model at the components prone to failure. The variable kinematic model is obtained within the framework of Carrera Unified Formulation, which was introduced by Carrera [22] to produce 3D-like solutions via higher-order 2D [23, 24] or 1D models [25, 26]. According to 1D CUF, which is the case of the present paper, the 3D displacement field can be expanded elegantly as the kinematic field over the cross section. Numerical accuracy can be improved by employing an arbitrary refinement of kinematics. In the past few years, various types of 1D CUF model have been developed based on different classes of expanding functions, which are listed as follows: Taylor Expansion (TE) [25], Lagrange Expansion (LE) [27], Chebyshev Expansions (CE) [28] and Hierarchical Legendre Expansion (HLE) [19, 29]. The above introduced 1D CUF models can be implemented based on Equivalent Single Layer (ESL) and Layer-Wise approaches, respectively, where ESL assumes a continuous and differentiable displacement function through the thickness direction and LW hypothesizes a continuous displacement function limited to the layer level.

The present multiscale work focuses on the exploitation of LE to build 1D models, endowing LW and CW abilities in a manner to face multiscale problems sraightforwardly. Carrera et al. [30] carried out a CW analysis for fiber-reinforced composites using 1D CUF-LE. 3D stress/displacement fields at different scales can be detected using the global model, i.e., full homogenized laminates, or partial local model, i.e., the combination of homogenized laminates and fiber-matrix constituents, or, full local model, i.e., only fiber-matrix constituents. Subsequently, exploiting CW capabilities, Maiarú et al. [31] extended 1D CUF-LE model for the prediction of failure parameters. Kaleel et al. [32] developed a novel and computationally efficient micromechanics framework based on 1D CUF-LE model to model components within RVEs. However, the aforementioned work is investigated in the domain of weak-form solutions, i.e. Finite Element Method (FEM). Navier-type solution, as a strong-form solution, can provide exact solution of structures under the simply supported boundary conditions and has been increasingly used for a wide range of structural analysis in conjunction with 1D CUF-LE model, including the free vibration of isotropic [33] and laminated beams [34] and static analysis of laminated beams [35]. In addition, Navier-type solutions have been also applied in the domain of CUF-TE models by Giunta et al. [36, 37].

To our best knowledge, this is the first time the same Navier-type close-form solution is proposed for the CW analysis of fiber-reinforced composites in a multiscale sense by means of 1D CUF-LE models. The rest of this paper is organized as follows: A brief introduction of 1D CUF theory is presented in Section

2. The governing equation with CUF fundamental nucleus is derived by applying the principle of virtual work in Section 3 with the assembly of global stiffness matrix and load vector in Section 3.1 and Section 3.2, respectively. Section 4 describes the LW and CW ability of the proposed model in detail. Three numerical cases are considered in Section 5. And finally, main conclusions are outlined in the last section.

2 1D CUF theory

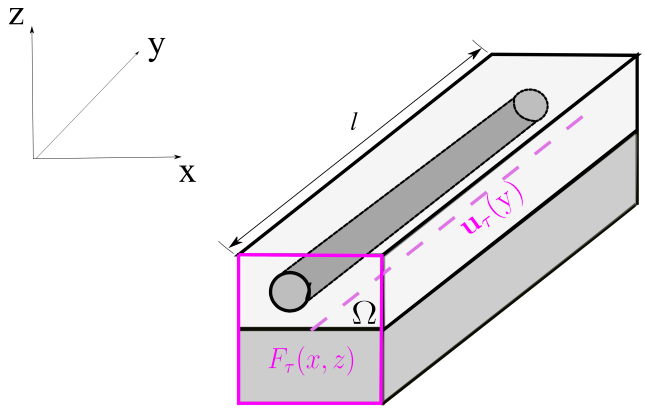

Figure 1: Coordinate systems for a beam with multi-components.

Traditional 1D beam theories do not work properly when an accurate analysis of structures with multi-components is required due to the deficiency in the kinematic description of the cross-sectional quantities and because non-classical phenomena may arise. To alleviate this drawback, 1D CUF could be considered as a competitive alternative. For the sake of an easy illustration, consider a two-layer composite beam in the Cartesian coordinate system with y-axis being the longitudinal axis in $0 \leq y \leq \mathrm{l}$ and xz-plane being the cross section Ω, as given in Fig. 1. The bottom layer is treated as the homogenized laminate and a fiber is embedded in the top layer around the matrix. This simple model is just a special case of more complex structures, i.e., an increasing number of fibers or laminates. Within the framework of CUF, the generic 3D displacement field can be expanded as any order of generic unknown variables over the cross section, which can be expressed as follows:

$$\mathbf{u}(x,y,z) = F_\tau(x,z)\mathbf{u}_\tau(y) \qquad \tau = 1,2,....,M \tag{1}$$

where F_τ are functions approximating the kinematic field over the cross section. $\mathbf{u}_\tau$ are the generalized displacements vector regarding axial coordinates y. M is the number of expanded terms, and τ stands for summation subscript.

From Eq. (1), one can see that the kinematic field of different components in a beam can be can be

modelled via a single formulation simultaneously. According to CUF-LE, displacement functions within each component can be constructed by a sum of the node displacement function elegantly. This feature enables a direct implementation of Layer-Wise [34] and Component-Wise [38] models by imposing the continuous displacement condition at the interface nodes. Four representative types of LE polynomials are often adopted, i.e., four-node bilinear L4, six-node biquadratic L6, nine-node biquadratic L9 and sixteen-node cubic L16. The function of L9 polynomial is given here for illustrative purposes:

$$
\begin{aligned}
&F_\tau = \tfrac{1}{4}(\mathrm{r}^2 + \mathrm{r}\ \mathrm{r}_\tau)(\mathrm{s}^2 + \mathrm{s}\ \mathrm{s}_\tau) \qquad \tau = 1,3,5,7 \\
&F_\tau = \tfrac{1}{2}\mathrm{s}_\tau^2(\mathrm{s}^2 - \mathrm{s}\ \mathrm{s}_\tau)(1 - r^2) + \tfrac{1}{2}\mathrm{r}_\tau^2(\mathrm{r}^2 - \mathrm{r}\ \mathrm{r}_\tau)(1 - \mathrm{s}^2) \qquad \tau = 2,4,6,8 \\
&F_\tau = (1 - \mathrm{r}^2)(1 - \mathrm{s}^2) \qquad \tau = 9
\end{aligned}
\tag{2}
$$

where r and s are defined over the interval $[-1, +1]$, and r_τ and s_τ are the coordinates of the nine points in the natural domain. For more details about the description of other kinds of LE polynomials, one can refer to the work by Carrera and Petrolo [27].

3 Principle of virtual work

The governing equations for a generic beam structure within the framework of Navier-type solution can be derived by means of principle of virtual work. For the static problem, it holds:

$$
\delta L_{\text{int}} = \delta L_{\text{ext}} \tag{3}
$$

where δ represents the symbol of a virtual variation. L_{int} is the strain energy, L_{ine} is the virtual work of the external loading.

The strain energy can be given as:

$$
\delta L_{\text{int}} = \int_l \int_{\mathbf{\Omega}} \delta \boldsymbol{\epsilon}^{\mathrm{T}} \boldsymbol{\sigma} \mathrm{d}\mathbf{\Omega} \mathrm{d}y \tag{4}
$$

where $\mathbf{\Omega}$ and l are the integration domain over the cross section and the length of the beam. Consider the geometrical relations and 3D constitutive law, as follows:

$$
\boldsymbol{\epsilon} = \mathbf{D}\mathbf{u}, \quad \boldsymbol{\sigma} = \tilde{\mathbf{C}}\boldsymbol{\epsilon} \tag{5}
$$

where $\mathbf{D}$ and $\tilde{\mathbf{C}}$ are 6×3 and 6×6 matrices. For the sake of brevity, one can find their explicit forms in [27]. Considering the CUF kinematic field in Eq. (1) and Eq. (5), Eq. (4) can be rewritten in a compact form after opportune integration by parts:

$$\delta L_{\text{int}} = \int_l (\delta \boldsymbol{u}_\tau)^{\mathrm{T}} \mathbf{K}^{\tau s} \boldsymbol{u}_s \mathrm{d}y + \left[(\delta \boldsymbol{u}_\tau)^{\mathrm{T}} \mathbf{\Pi}^{\tau s} \boldsymbol{u}_s\right] |_{y=0}^{y=l} \tag{6}$$

where $\mathbf{K}^{\tau s}$ and $\mathbf{\Pi}^{\tau s}$ are the fundamental nuclei of the stiffness matrix and the matrix of natural boundary conditions, which are reported in the book from Carrera et al. [39]. It is possible to demonstrate that the term containing $\mathbf{\Pi}^{\tau s}$ is automatically satisfied in the case of simply supported boundary condition.

The virtual variation of the external work done by the surface load $\mathbf{p_{ij}^{n\pm}}, i,j = x,y,z$ imposed on the nth sub-domain on the cross section, can be expressed as:

$$\delta L_{\text{ext}} = \left(\delta L_{\mathbf{p_{xx}^{n\pm}}} + \delta L_{\mathbf{p_{xy}^{n\pm}}} + \delta L_{\mathbf{p_{xz}^{n\pm}}} + \delta L_{\mathbf{p_{zx}^{n\pm}}} + \delta L_{\mathbf{p_{zy}^{n\pm}}} + \delta L_{\mathbf{p_{zz}^{n\pm}}}\right) \tag{7}$$

For the sake of brevity, only the expression of $\delta L_{\mathbf{p_{zz}^{n\pm}}}$ is reported here:

$$\delta L_{\mathbf{p_{xx}^{n\pm}}} = \int_l \delta u_{z\tau} \mathbf{p_{zz}^{n\pm}} E_\tau^{nx^\pm} \, dy, \quad \left(E_\tau^{nx^+}, E_\tau^{nx^-}\right) = \int_{x_1^n}^{x_2^n} \left(F_\tau\left(z_2^n, x\right), F_\tau\left(z_1^n, x\right)\right) \, dx \tag{8}$$

$\left[z_1^k, z_2^k\right]$ indicate the z coordinates of the bottom and upper surfaces, respectively. The explicit expressions of the other components in Eq. (7) can be found in [39].

3.1 Navier-type solution

Based on the assumption of Navier-type solution, the displacement fields and transverse surface load can be expressed as a sum of harmonic functions:

$$\begin{gathered} u_{xs}(y) = U_{xs}\sin(\alpha y) \\ u_{ys}(y) = U_{ys}\cos(\alpha y) \\ u_{zs}(y) = U_{zs}\sin(\alpha y) \\ \mathbf{p_{ij}^{n\pm}} = \left\{ \begin{array}{c} p_{xx}^{n\pm}\sin(\alpha y), p_{xy}^{n\pm}\cos(\alpha y), p_{xz}^{n\pm}\sin(\alpha y), \\ p_{zx}^{n\pm}\sin(\alpha y), p_{zy}^{n\pm}\cos(\alpha y), p_{zz}^{n\pm}\sin(\alpha y) \end{array} \right\} \end{gathered} \tag{9}$$

where α is:

$$\alpha = \frac{m\pi}{l} \tag{10}$$

and $U_{x\tau}$, $U_{y\tau}$ and $U_{z\tau}$ are amplitudes of the generalized displacement components. l is the length of the beam. m is the half wave number along the beam axis.
Considering Eq. (9) and Eq. (3), one can obtain the governing equation as:

$$\mathbf{K}^{\tau s}\boldsymbol{U}^{\boldsymbol{s}} = \mathbf{P}^{\tau} \tag{11}$$

The explicit expressions of the stiffness matrix $\mathbf{K}^{\tau s}$ and load vector $\mathbf{P}^{\tau}$ have been given in [35].

3.2 FE approach

As an alternative approach, FE approach has long been used to obtain approximate solutions of displacements and stresses, which are included in this paper for comparison reasons. In 1D CUF-FEM, the generalized displacements $\mathbf{u}_{\tau}$ are interpolated along the beam y-axis utilizing the shape functions N_i, as shown in Eq. (12)

$$\mathbf{u}_{\tau}(y) = N_i(y)\mathbf{u}_{\tau i} \qquad i = 1, 2, ..., n \tag{12}$$

where $\mathbf{u}_{\tau i} = \{u_{x_{\tau i}} u_{y_{\tau i}} u_{z_{\tau i}}\}$ are the node unknown displacements. i is the the number of node per element in the case of Lagrangian shape functions. Four-node 1D element is herein adopted to improve convergence speed and reduce computational cost, whose expression is a cubic-order polynomial in terms of y variable and can be found in [40].
Combining Eq. (12) and Eq. (3), one has:

$$\mathbf{K}^{\tau sij}\boldsymbol{U}^{sj} = \mathbf{P}^{\tau i} \tag{13}$$

The detailed information of the stiffness matrix $\mathbf{K}^{\tau sij}$ and load vector $\mathbf{P}^{\tau i}$ of the CUF-FEM can be found in [41].

4 Multiscale analysis of composites

Eq. (11) and Eq. (13) are written at the component level. Composition of fiber, matrix or homogenized laminates can be assembled into a global matrix using the CW approach. To be specific, the global matrix can be obtained by the contribution of LE expansions on the cross-section sub-domain in each component, and the matrix elements of the shared kinematics at the interface between different components should be superposed to assure the continuity of the displacement solutions, enabling the construction of CW analysis straightforwardly. In the case of Navier-type solution, prismatic bodies can be analysed by systematically solving a linear system of algebraic equations via exact closed-form solution. Similarly, in terms of FE approach, global matrices needs to be expanded and eventually assembled along the beam axis direction. For

the sake of illustration, Fig. 2 presents the contructions of the stiffness matrix for the multi-scale and CW analysis of a fibre/matrix laminate. In detail, the figure shows the case of both Navier-type approach and FEM for a L4 expansion above the cross-section of each component. In the case of FEM, moreover, a single four-node cubic finite element along the beam axis is considered in the picture. It should be underlined that the main novelty of this work is the development of CW closed-form solution for the multiscale analysis of composites. FEM approximation is used hereinafter for comparison purposes.

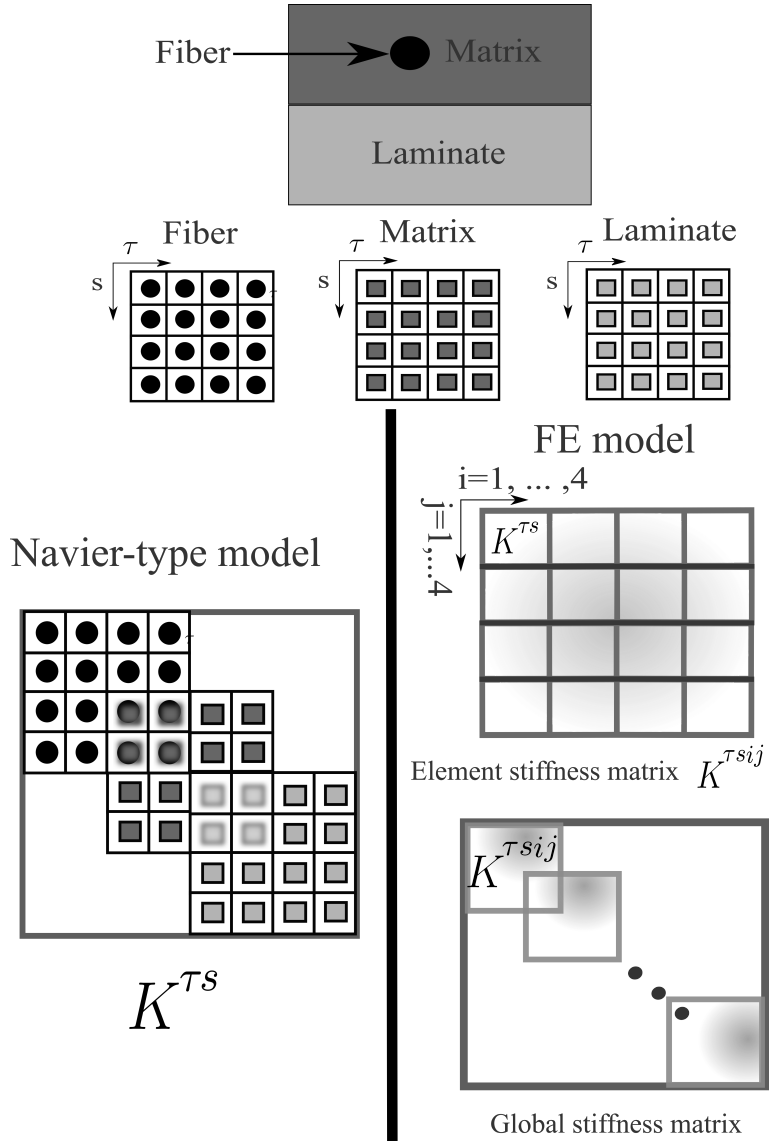

Figure 2: Comparison of assembly process between Navier-type and FE models in a two-layer laminated beam via multiscale CW approach.

5 Numerical results

In the current section, numerical examples are performed on three different structures under the simply-supported boundary condition by means of multiscale analysis via the CUF-LE formulation. First, a single-

layer composite beam is considered, followed by multi-layered composite and sandwich beams.

5.1 Single-layer transversely isotropic beam

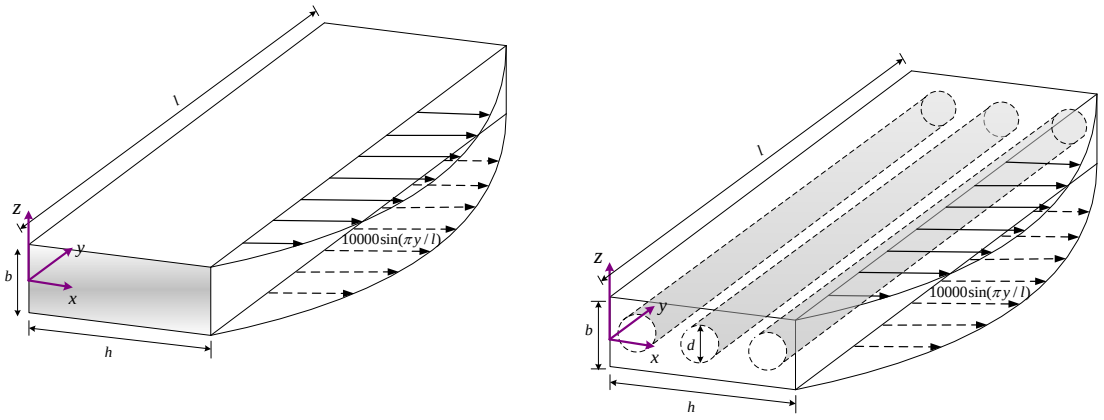

(a) MAM (b) MIM

Figure 3: Multiscale model for a transversely isotropic beam under sinusoidal pressure load

As the first assessment, a transversely isotropic beam is selected to test the capabilities of the present CUF-CW method. Macro-scale (MAM) and micro-scale (MIM) Models are provided in Fig. 3 with a 3D view of this case. MAM is regarded as a homogenized medium, while MIM is treated as a fiber-matrix composition to mimic the mechanics of each component. The characteristic dimensions of the structure are: width, $b = 1/15$m, height, $h = 0.2$m, and slenderness ratio, $l/h = 10$. The fiber diameter is $d = 0.056$m in the MIM. Material properties for different components in the material coordinate system (1,2,3) are given in Table 1. To be specific, the fiber is assumed to be transversely isotropic, and the matrix is isotropic. For comparison purposes, material properties of the homogenized cell are calculated from those of the corresponding fiber and matrix by means of rule of mixture. A transverse sinusoidal loading is applied at the face $[h, :, :]$ with regard to $q(y) = p_0 \sin \frac{\pi y}{l}$ Pa with p_0 equal to 10000. All the results are given in the following dimensionless form:

$$\bar{u}_i = \frac{E_2}{h} u_i \quad \text{with} \quad i = x, y; \quad \bar{u}_z = 100 \frac{E_2 h^3}{l^4} u_z$$
$$\bar{\sigma}_{ij} = \frac{\sigma_{ij}}{p_0} \quad \text{with} \quad i = x, y, z; \quad \bar{z} = \frac{z}{h} \tag{14}$$

where $\bar{u}_i$ and $\bar{\sigma}_{ij}$ stand for the dimensionless displacement and stress components.

Table 2 presents the non-dimensional results regarding displacements ($\bar{u}_x$, $\bar{u}_y$) and stresses ($\bar{\sigma}_{yy}$, $\bar{\sigma}_{yz}$) at representative locations for different-scale models. For each-scale model, CUF closed-form (Navier) solutions are compared to FEM solutions, which make use of $16B4$ beam elements along the y-axis. The enhanced capability of CUF FEM solutions has been validated comprehensively in Ref.[38] and, therefore, serving as

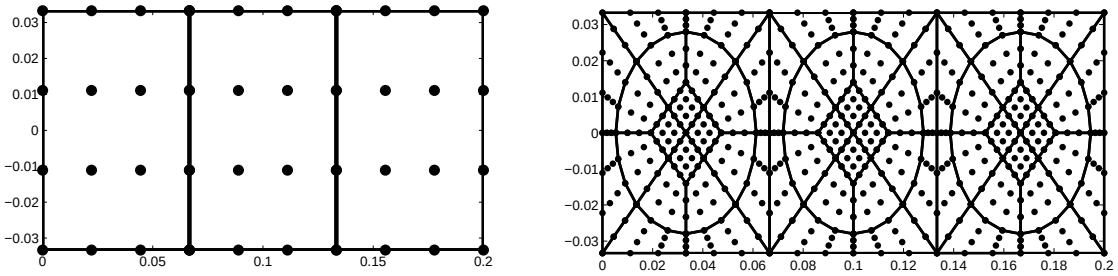

(a) 3×1 L16 cross-sectional distribution for MAM (b) 60 L16 cross-sectional distribution for MIM

Figure 4: Two different cross-sectional models

Table 1: Material properties for different components of a transversely isotropic beam

Component	E_1 (Pa)	E_2 (Pa)	E_3 (Pa)	G_{12} (Pa)	G_{13} (Pa)	G_{23} (Pa)	ν_{12}	ν_{13}	ν_{23}
Fiber	4.44×10^{11}	1.16×10^{10}	1.16×10^{10}	8.67×10^{9}	8.67×10^{9}	4.80×10^{9}	0.21	0.21	0.21
Matrix	8.55×10^{9}	8.55×10^{9}	8.55×10^{9}	3.28×10^{9}	3.28×10^{9}	3.28×10^{9}	0.31	0.31	0.31
lamina	2.50×10^{11}	1.00×10^{10}	1.00×10^{10}	5.00×10^{9}	5.00×10^{9}	2.00×10^{9}	0.25	0.25	0.25

Table 2: Non-dimensional displacement and stress values of a transversely isotropic beam for different models, $l/b = 10$.

Model	$\bar{u}_x$	$\bar{u}_y$	$\bar{\sigma}_{yy}$	$\bar{\sigma}_{xy}$	DOFs
	$[h/3, l/2, 0]$	$[2h/3, 0, 0]$	$[h/6, l/2, 0]$	$[5h/6, 0, 0]$	
MAM-Exact solution					
A: 3×1 L4	0.714	-2.246	-40.351	2.508	24
B: 3×1 L9	0.734	-2.349	-39.241	2.509	63
C: 3×1 L16	0.734	-2.351	-39.291	2.711	120
MAM-FE solution					
A: 3×1 L4	0.713	-2.220	-40.314	2.524	1176
B: 3×1 L9	0.732	-2.231	-39.232	2.510	3087
C: 3×1 L16	0.733	-2.313	-39.278	2.715	5880
MIM-Exact solution					
A: 24 L6+28 L9	0.763	-2.608	-74.777	2.962	567
B: 60 L16	0.756	-2.570	-73.784	3.198	1695
MIM-FE solution					
A: 24 L6+28 L9	0.762	-2.570	-74.990	2.965	27783
B: 60 L16	0.754	-2.533	-73.986	3.145	52545

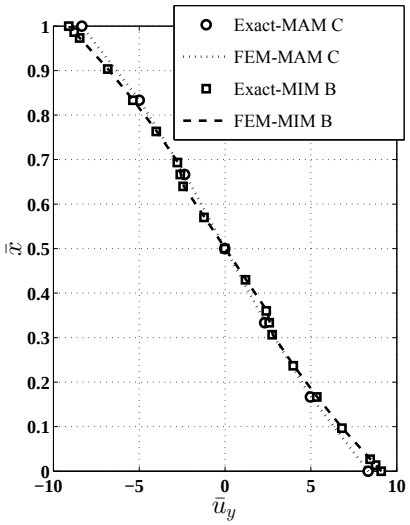

(a) $\bar{u}_y$ at $(y, z) = (0, 0)$

Figure 5: Non-dimensional axial displacement, $\bar{u}_y$, single-layer beam.

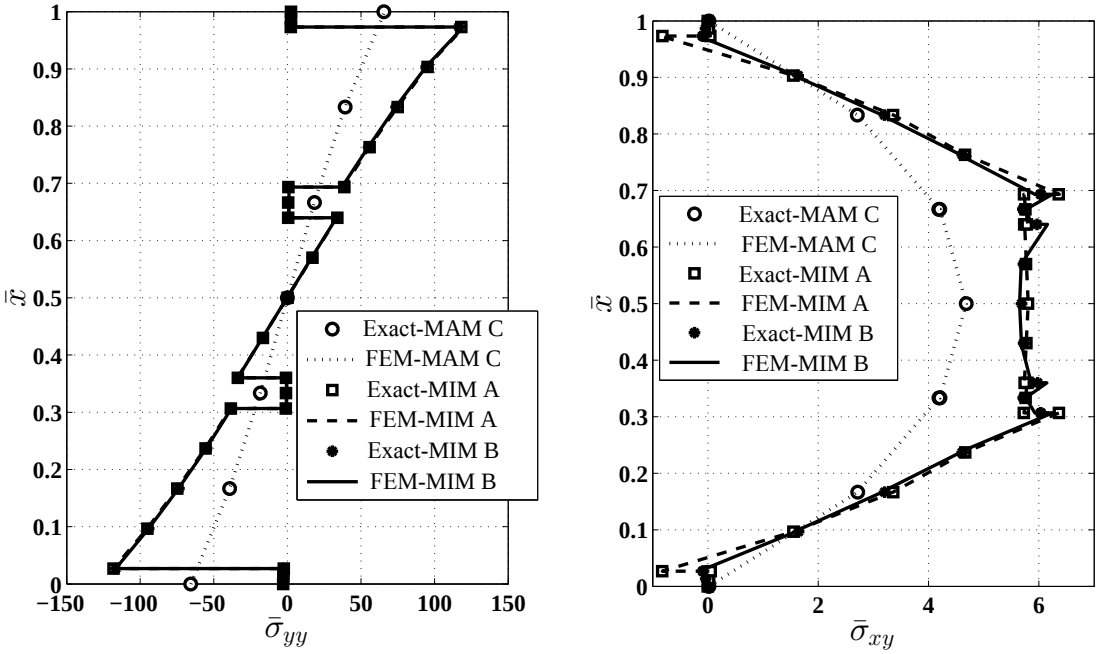

(a) $\bar{\sigma}_{yy}$ at $(y, z) = (l/2, 0)$

(b) $\bar{\sigma}_{xy}$ at $(y, z) = (0, 0)$

Figure 6: Non-dimensional axial stresses, $\bar{\sigma}_{yy}$ and transverse shear stress, $\bar{\sigma}_{xy}$, single-layer beam.

reference solutions in the present paper. In Table 2, the first column represents the type of the CUF-LE model and the last column represents the number of degrees of freedom (DOFs) for each model. For the sake of brevity, we just give two CUF-LE cross-sectional distributions in Fig. 4 for illustrative purposes. Interested readers can refer to Pagani et al. [35] for the detailed description of each type of the model. Results over the end-side and midspan cross sections along the thickness direction are shown in Fig. 5 and Fig. 6 with regard to non-dimensional axial displacement, axial stress and transverse shear stress, respectively. In addition, Fig.

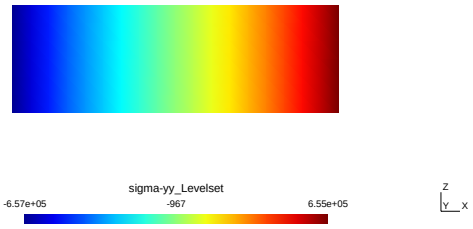

(a) Exact-MAM C, σ_{yy}

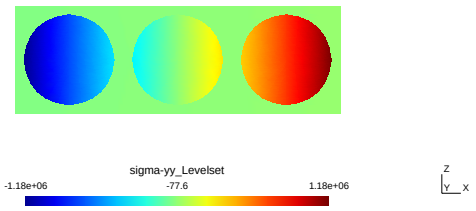

(b) Exact-MIM B, σ_{yy}

Figure 7: Comparison of axial stresses, σ_{yy} for two different-scale models at cross section $[:, l/2, :]$.

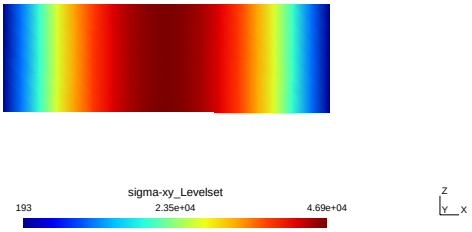

(a) Exact-MAM C, σ_{xy}

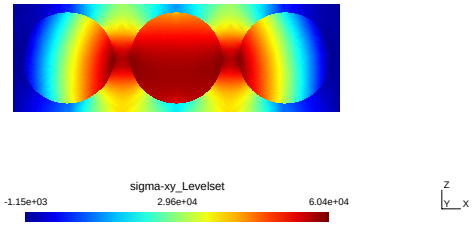

(b) Exact-MIM B, σ_{xy}

Figure 8: Comparison of shear stresses, σ_{xy} for two different-scale models at cross section $[:, 0, :]$.

7 and Fig. 8 depict a direct comparison of stresses ($\bar{\sigma}_{yy}$ and $\bar{\sigma}_{xy}$) between MAM and MIM for different closed-form solutions of the mentioned CUF models. Through the present assessment, the following conclusion can be reached:

1. FE and exact closed-form solutions of CUF models are in good agreement for both MAM and MIM with a significant reduction in computational cost in Table 2.

2. Displacement values, computed by MAM and MIM, show less difference compared with stress values, especially for axial stress solution. Therefore, MAM is suggested for the detection of displacement fields for saving computational costs, in this special analysis case.

3. According to distributions in Fig. 5 and Fig. 6, it is possible to see that MAM cannot describe the mechanical behavior of fiber and matrix, which is even worse for axial stress due to the simplified homogeneous properties introduced in the corresponding layer. On the other hand, concerning MIM, quadratic 24 L6+28 L9 fails to capture the interface continuity of the shear stress. Higher-order model with enough DOFs (60 L16) is adequate enough to retrieve the continuous shear stress fields.

5.2 Cross-ply laminated beam

This section performs a multiscale analysis of a three-layer [0°/90°/0°] cross-ply laminated beam. Three different-scale models, i.e., Meso-scale Model (MEM), MIM 1 and MIM 2 are selected, whose cross-sectional configurations are displayed in Fig. 9. In MEM, homogenized material properties are assumed for each layer; in MIM 1 and 2, the fiber and matrix are modelled separately for the bottom layer and both of the top and bottom layer. The aim of the analysis is to reveal more complex mechanical characteristics of interfaces between different components. Each layer is of the same thickness with value $h/3 = 1/15$m, Other characteristic dimensions, material properties of different components are the same as those in the previous case. The transverse sinusoidal loading is applied on the top face with $q(y) = \sin \frac{\pi y}{l}$ Pa.

Numerical results concerning non-dimensional displacements $\bar{u}_z$ ($[0, l/2, -h/2]$), $\bar{u}_y$ ($[0, 0, -h/2]$) and non-dimensional stresses $\bar{\sigma}_{yy}$ ($[b/2, l/2, 0]$), $\bar{\sigma}_{yz}$ ($[b/2, 0, -h/3]$) obtained from present LE-close-form model with various approximations of the cross-section kinematics are given in Table 3. 1D CUF FEM solutions, the Exact Solution for the Cylindrical Bending of Plates (ESCBP) developed by Pagano [42], the Beam Layer-Wise Theory (BLWT) employed by Tahani [43] and the 3D ABAQUS model are also shown in this table for comprehensive comparisons along with DOFs. 1D CUF $16B4$ beam elements along the $y-axis$ and 3D brick element C3D20 ($15 \times 40 \times 15$) are selected from convergence analysis. To make a further comparison of the solutions among MEM, MIM 1 and MIM 2, Fig. 10 and Fig. 11 show the distribution of these variables across the thickness of the layer at two specific locations. Stress maps over the surface are plotted in Fig. 12

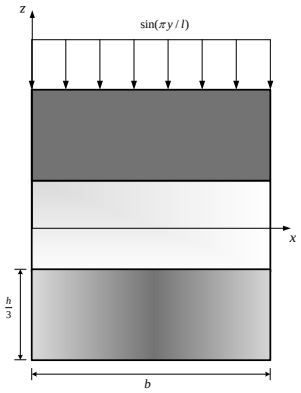

(a) The cross section for MEM

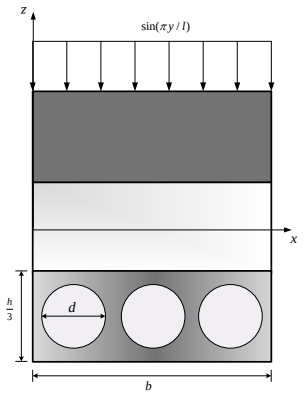

(b) The cross section for MIM 1

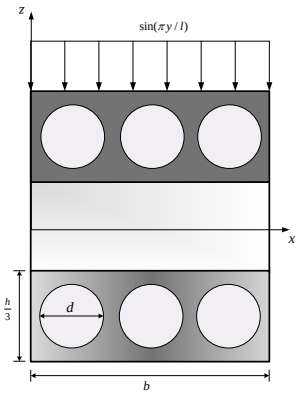

(c) The cross section for MIM 2

Figure 9: Three different cross-sectional configurations of a cross-ply laminated beam.

and Fig. 13, in which, the reader can have an intuitive appreciation for the diversity of three-scale models. Through the present example, the following comments can be made:

1. The solutions for three-scale models provided by the proposed exact solutions are in perfect agreement with those of ABAQUS, FE models of CUF and the literature with lower computational cost. In the case of MEM, closed-form solution employs a maximum of 300 DOFs, with equivalent FE model having 14700 DOFs and ABAQUS 3D 197496 DOFs, as shown in Table 3. On the other hand, displacement values presents a faster convergence rate than stress components for all the models.

2. MIM 2 gives a perfect description of displacements and stresses regardless of fibers, matrices and middle laminates. However, in order to fulfill the continuity condition of the shear stress in the fiber-matrix contact area, L16 model with enough cross-sectional discretization is required, accompanied by the increasing computational cost in the case of FE method. This means that if an accurate CUF-FEM mechanical analysis is needed at the given fibers (Fig.12(b)), the adoption of fiber-matrix cell is recommended around the area where needed with the use of L16 model, making an excellent compromise

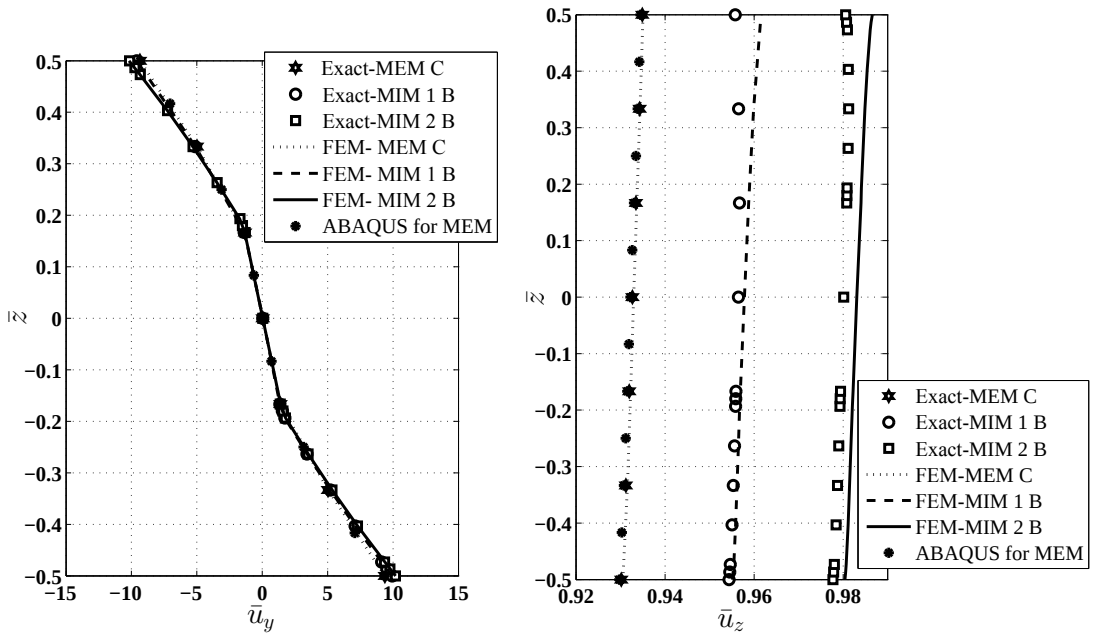

(a) $\bar{u}_y$ at $(x, y) = (b/2, 0)$ (b) $\bar{u}_z$ at $(x, y) = (b/2, l/2)$

Figure 10: Non-dimensional axial displacements, $\bar{u}_y$ and transverse displacements, $\bar{u}_z$ for the various multiscale models of the three-layer beam.

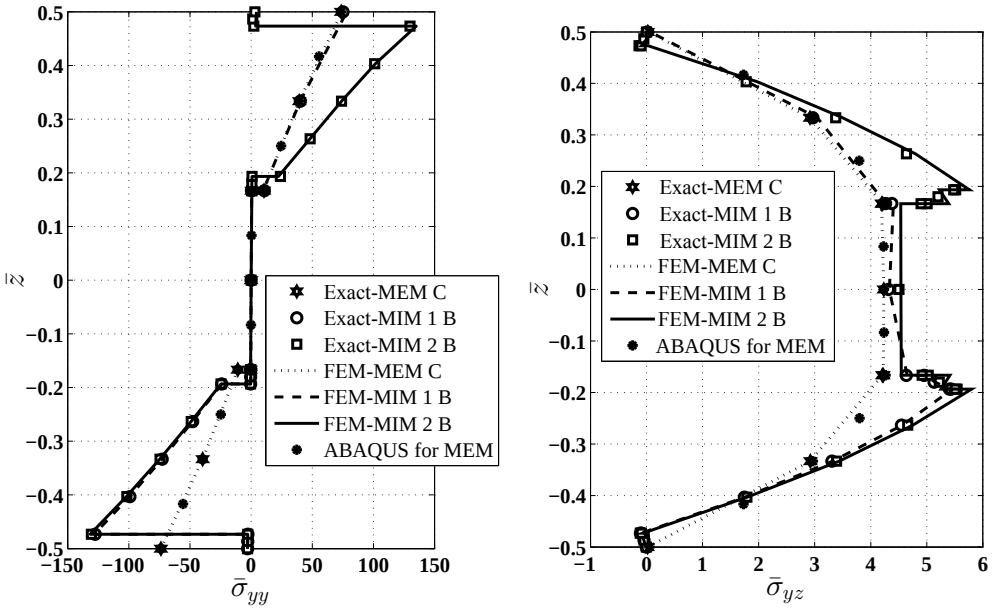

(a) $\bar{\sigma}_{yy}$ at $(x, y) = (b/2, l/2)$ (b) $\bar{\sigma}_{yz}$ at $(x, y) = (b/2, 0)$

Figure 11: Non-dimensional axial stresses, $\bar{\sigma}_{yy}$ and transverse shear stresses, $\bar{\sigma}_{yz}$ for the various multiscale models of the three-layer beam.

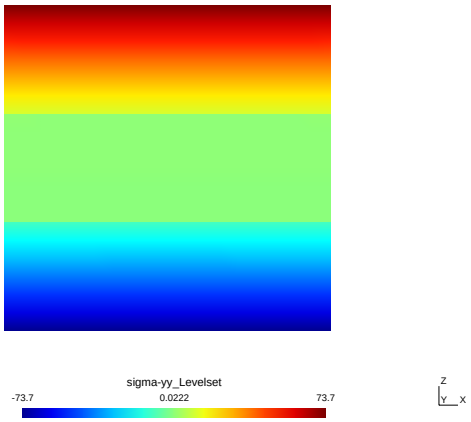

(a) Exact-MEM C, $\bar{\sigma}_{yy}$

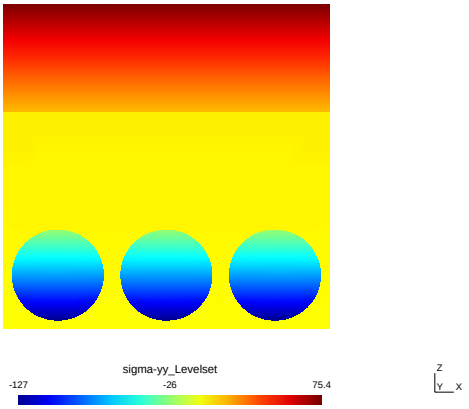

(b) Exact-MIM 1 B, $\bar{\sigma}_{yy}$

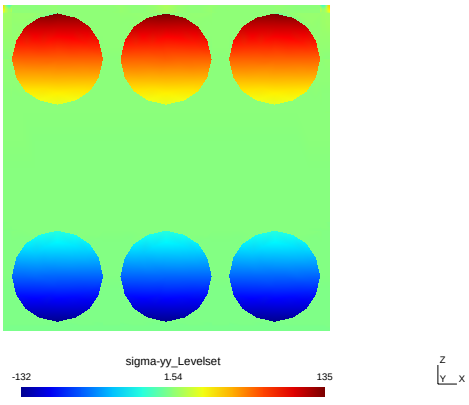

(c) Exact-MIM 2 B, $\bar{\sigma}_{yy}$

Figure 12: Comparison of the dimensionless axial stresses, $\bar{\sigma}_{yy}$ for three different-scale models at cross section $[:, l/2, :]$.

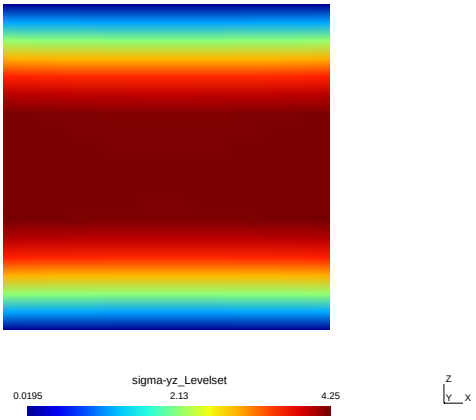

(a) Exact-MEM C, $\bar{\sigma}_{yz}$

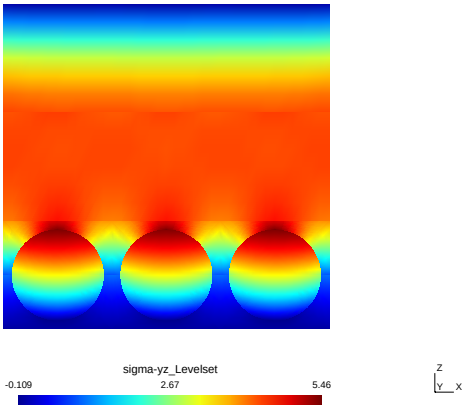

(b) Exact-MIM 1 B, $\bar{\sigma}_{yz}$

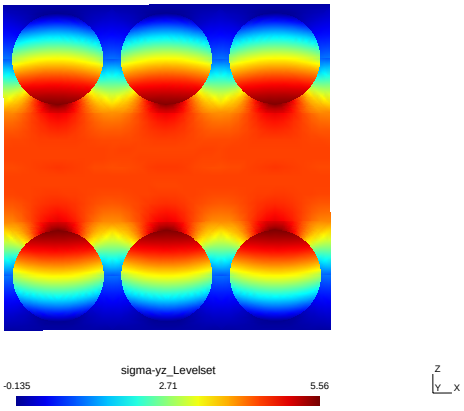

(c) Exact-MIM 2 B, $\bar{\sigma}_{yz}$

Figure 13: Comparison of the dimensionless shear stresses, $\bar{\sigma}_{yz}$ for three different-scale models at cross section $[:, 0, :]$.

Table 3: Non-dimensional displacement and stress values of a cross-ply laminated beam for different models, $l/b = 10$.

Model	$\bar{u}_z$	$\bar{u}_y$	$\bar{\sigma}_{yy}$	$\bar{\sigma}_{yz}$	DOFs
	$[0, l/2, -h/2]$	$[0, 0, -h/2]$	$[b/2, l/2, 0]$	$[b/2, 0, -h/3]$	
Reference solutions for MEM					
ESCBP [42]	0.920	9.300	–	–	–
BLWT [43]	0.900	–	–	–	–
FEM 3D[a]	0.931	9.369	0.108	2.967	197496
MEM-Exact solution					
A: 3×3 L4	0.911	9.038	0.108	2.648	48
B: 3×3 L9	0.931	9.353	0.109	2.656	147
C: 3×3 L16	0.932	9.363	0.109	2.922	300
MEM-FE solution					
A: 3×3 L4	0.912	9.043	0.092	2.648	2352
B: 3×3 L9	0.931	9.358	0.093	2.656	7203
C: 3×3 L16	0.932	9.368	0.094	2.924	14700
MIM 1-Exact solution					
A: 24 L6+48 L9	0.958	10.051	0.098	3.532	819
B: 72 L16	0.957	9.995	0.059	3.310	2037
MIM 1-FE solution					
A: 24 L6+48 L9	0.959	10.061	0.068	3.529	40131
B: 72 L16	0.957	10.005	0.083	3.321	38703
MIM 2-Exact solution					
A: 48 L6+66 L9	0.980	10.328	0.097	3.627	1197
B: 132 L16	0.986	10.237	0.108	3.391	3846
MIM 2-FE solution					
A: 48 L6+66 L9	0.987	10.339	0.071	3.626	58653
B: 126 L9	0.982	10.272	0.083	3.438	30039

[a]: The number of elements is $15 \times 40 \times 15$

between accuracy and computational cost. Conversely, a Navier-type solution can easily overcome the above limitations of computational efficiency and provide results with high accuracy at arbitrary scale with acceptable DOFs elegantly (Fig. 10 and Fig. 11).

5.3 Sandwich beam

To test the component-wise ability of the present 1D models on heterogeneous structures with different material properties, a sandwich beam is chosen as the last analysis case. Following the global-local modelling procedure as in the first two cases, MEM supposes all the layers with homogenized material properties and MIM assumes the bottom layer as a fiber-matrix cell, as shown in Fig. 14. Its geometric dimensions are considered as follows: width $b = 0.04m$, height $h = 0.12m$ and length-to-height ratio $l/h = 10$. The top and bottom faces have the same thickness: $h/6 = 0.02m$. To build a more reasonable MIM model, eight fibers

with each of fiber diameter $d = 0.008$m are accounted for the present assessment. Table 4 shows material properties of four components, i.e., fiber, matrix, soft core and top face, where the homogenized properties in the top layer are obtained via rule of mixtures. The transverse sinusoidal loading is applied on the top face with $q(y) = \sin \frac{\pi y}{l}$ Pa.

Table 4: Material properties for each component of the sandwich beam

Component	E_1 (Pa)	E_2 (Pa)	E_3 (Pa)	G_{12} (Pa)	G_{13} (Pa)	G_{23} (Pa)	ν_{12}	ν_{13}	ν_{23}
Fiber	4.44×10^{11}	1.16×10^{10}	1.16×10^{10}	8.67×10^{9}	8.67×10^{9}	4.80×10^{9}	0.21	0.21	0.21
Matrix	8.55×10^{9}	8.55×10^{9}	8.55×10^{9}	3.28×10^{9}	3.28×10^{9}	3.28×10^{9}	0.31	0.31	0.31
Core	2.21×10^{5}	2.00×10^{5}	2.76×10^{9}	1.66×10^{6}	5.45×10^{8}	4.55×10^{8}	0.99	3.00E-05	3.00E-05
Top face	2.28×10^{11}	9.85×10^{9}	9.85×10^{9}	4.77×10^{9}	4.77×10^{9}	3.92×10^{9}	0.26	0.26	0.26

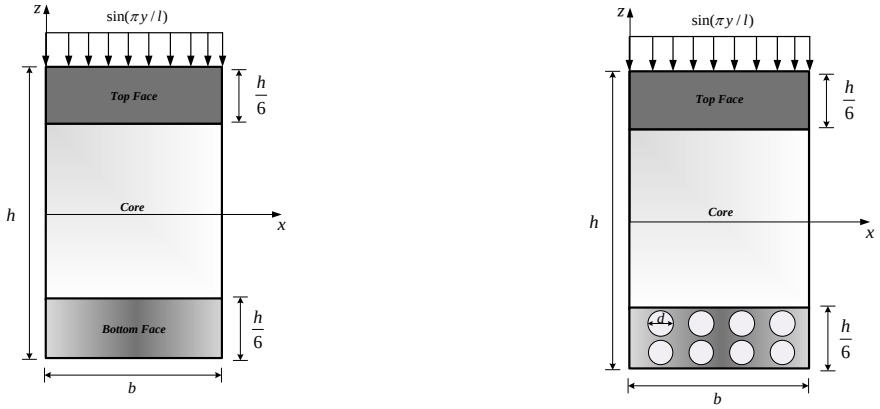

(a) The cross section for MEM

(b) The cross section for MIM

Figure 14: Cross-sectional configurations of a sandwich beam at different scales.

Table 5 compares the numerical solutions in terms of displacements and stresses at some representative points predicted by different models. Fig. 17 and Fig. 18 show a detailed comparison of the distribution of axial and shear stresses over the surface of the section ($[:, l/2, :]$ and $[:, 0, :]$) modelled by MEM and MIM, respectively. In particular, the reader can find the plots of these displacements and stresses across the thickness of the corresponding cross section in Fig. 15 and Fig. 16. The analysis of the results suggest the following considerations:

1. One can notice the results by CUF closed-form solutions are in high agreement of those by FEM. It is worth noting that the transverse displacements $\bar{u}_z$ predicted by different models show better consistency than other variables, as shown in Table 5. Besides, the axial stress solution of the point in the

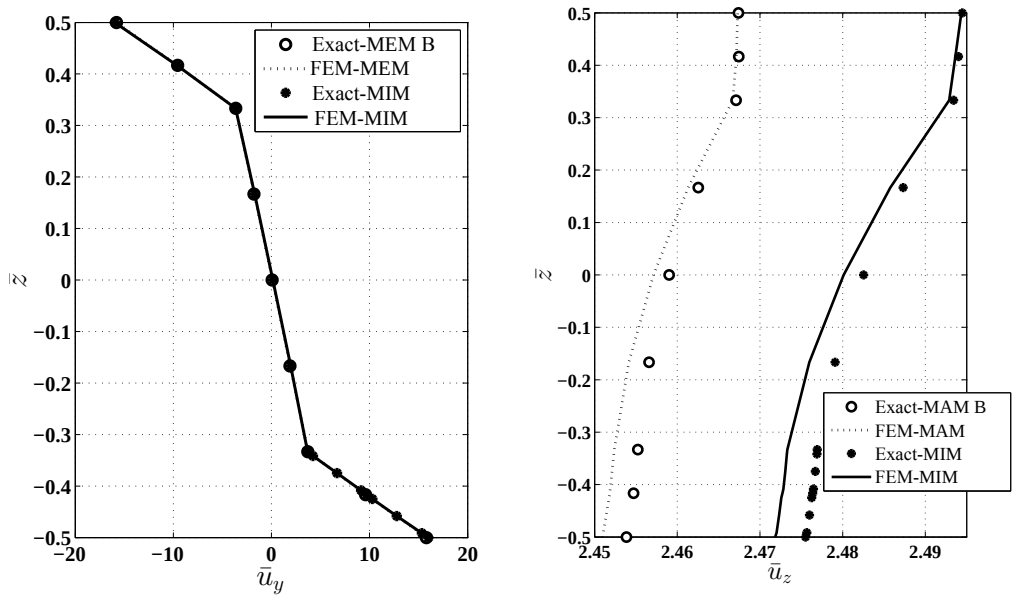

(a) $\bar{u}_y$ at $(x, y) = (b/2, 0)$ (b) $\bar{u}_z$ at $(x, y) = (b/2, l/2)$

Figure 15: Non-dimensional axial displacements, $\bar{u}_y$ and transverse displacements, $\bar{u}_z$ for all the CUF models of the sandwich beam.

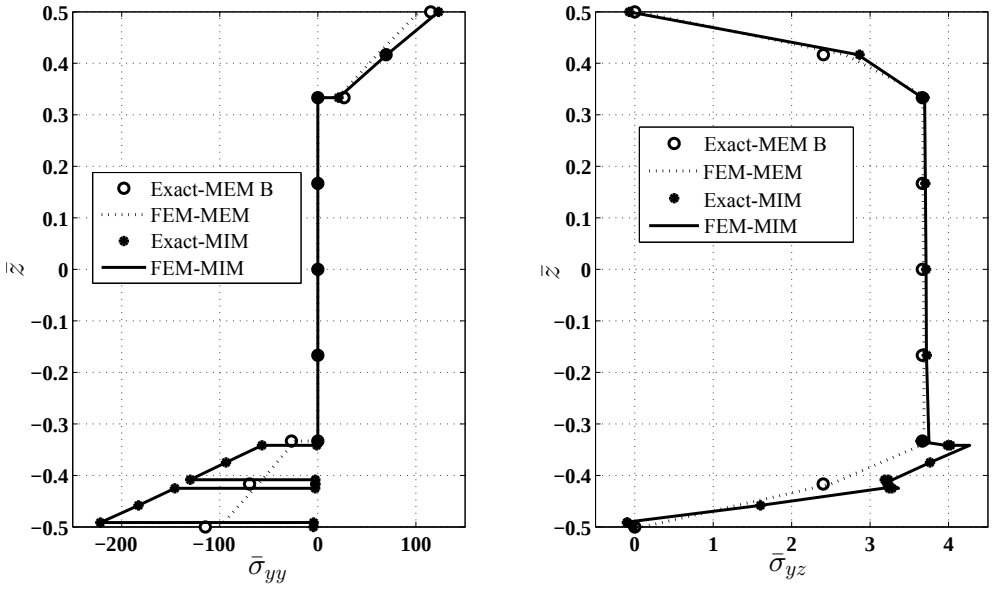

(a) $\bar{\sigma}_{yy}$ at $(x, y) = (b/2, l/2)$ (b) $\bar{\sigma}_{yz}$ at $(x, y) = (b/2, 0)$

Figure 16: Non-dimensional axial stresses, $\bar{\sigma}_{yy}$ and transverse shear stresses, $\bar{\sigma}_{yz}$ for all the CUF models of the sandwich beam.

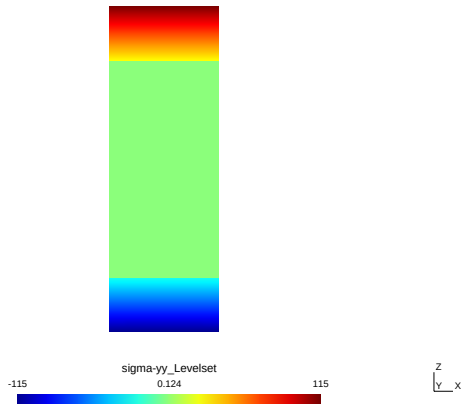

(a) Exact-MEM B, $\bar{\sigma}_{yy}$

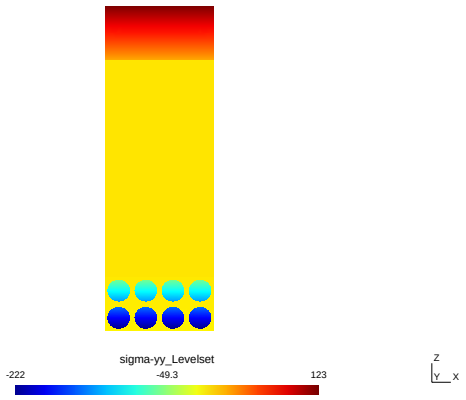

(b) Exact-MIM, $\bar{\sigma}_{yy}$

Figure 17: Comparison of the dimensionless axial stresses, $\bar{\sigma}_{yy}$ for two models at cross section $[:, l/2, :]$.

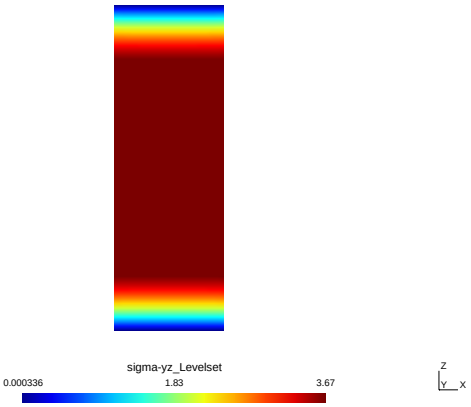

(a) Exact-MEM B, $\bar{\sigma}_{yz}$

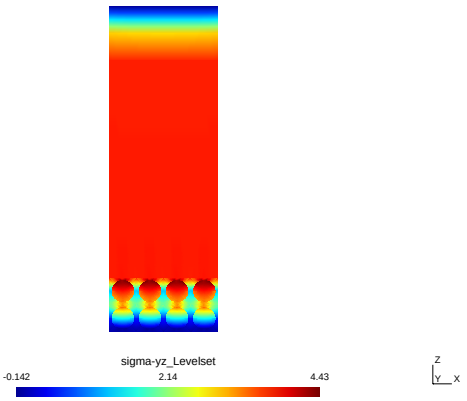

(b) Exact-MIM, $\bar{\sigma}_{yz}$

Figure 18: Comparison of the dimensionless shear stresses, $\bar{\sigma}_{yz}$ for two models at cross section $[:, 0, :]$.

Table 5: Non-dimensional displacement and stress values of a three-layer sandwich beam for different models, $l/b = 10$.

Model	$\bar{u}_z$	$\bar{u}_y$	$\bar{\sigma}_{yy}$	$\bar{\sigma}_{yz}$	DOFs
	$[0, l/2, -h/2]$	$[0, 0, -h/2]$	$[b/2, l/2, 5h/12]$	$[b/2, 0, -h/3]$	
MEM-Exact solution					
A: 4×8 L9	0.025	15.979	69.654	3.758	459
B: 4×8 L16	0.025	15.797	69.650	3.666	975
MEM-FE solution					
4×8 L9	0.025	15.837	69.820	3.774	8721
MIM-Exact solution					
272 L16	0.025	16.015	69.927	3.736	7509
MIM-FE solution					
208 L9	0.025	15.995	70.326	3.789	33891

homogenized layer shows smaller discrepancies than that in the fiber-matrix cell, referring to the first case when global-local analysis is performed.

2. Due to the adoption of a more complex MIM, an increasing computation cost is required in the analysis at each scale. This drawback is eliminated by exact closed-form solutions of higher-order L16 models, which provides a continuous distribution of shear stress at the interfaces between different components. FEM models of refined CUF models within the framework of L9 fails in the correct representation of this issue, as shown in Fig. 16(b). On the other hand, it is possible to see an interesting phenomenon of the maximum axial stress in the lower fibers and maximum shear stress in the top fibers in Fig. 17(b) and Fig. 18(b). Such local mechanical behaviors do not appear in MEM, as shown in Fig. 17(a) and Fig. 18(a)

6 Conclusions

In the present article, a unified exact solution is extended to the multiscale analysis of laminated and sandwich beams based on Carrera Unified Formulation (CUF). This novel CUF model enables a straightforward structural modelling in a component-wise sense due to the employment of cross-sectional description of the kineatics by Lagrange polynomials (Lagrange Expansion, LE). The utilization of CUF-LE allows the capability of the multiscale model through arbitrary combinations of different structural components (laminates, fibers and matrices). The numerical assessment of the proposed model has been performed by studying three typical composite structures. The following considerations arise from the obtained results:

1. CUF-close-form solutions can provide accurate stress/displacement results in high agreement with those of CUF-FEM with a significant reduction of computational cost.

2. Displacements predicted by models at different scales exhibit a higher level of consistency than stresses, that is, micro-scale model is recommended for the detection of stress fields. On the other hand, Macro-scale and Meso-scale Models may be suggested for the calculation of displacements for the analysis cases considered in the present research.

3. A continuous distribution of shear stress at the interface between different components can be efficiently described by higher-order model, e.g., L16 expansion. Besides, the use of L16 in mirco-scale model with CUF-FEM will lead to higher computational efforts. Thus, the partial micro-scale model is an alternative approach for the balance of the desired accuracy and computation cost, which means fiber-matrix cell is desired to be selected where failure may take place, in a pure multi-scale sense.

Acknowledgments

The first author acknowledges the support by the scholarship from the China Scholarship Council (CSC) (Grant No. 201606710014) and Fundamental Research Funds for the Central Universities (Grant No. 2014B31414).

References

[1] S. W. Tsai, Theory of composites design, Think composites Dayton, 1992.

[2] Y. Yan, Q. W. Ren, N. Xia, L. F. Zhang, A close-form solution applied to the free vibration of the euler–bernoulli beam with edge cracks, Archive of Applied Mechanics 86 (9) (2016) 1633–1646.

[3] D. Zhang, A. M. Waas, C.-F. Yen, Progressive damage and failure response of hybrid 3d textile composites subjected to flexural loading, part ii: mechanics based multiscale computational modeling of progressive damage and failure, International Journal of Solids and Structures 75 (2015) 321–335.

[4] F. Tornabene, M. Bacciocchi, N. Fantuzzi, J. Reddy, Multiscale approach for three-phase cnt/polymer/fiber laminated nanocomposite structures, Polymer Composites.

[5] R. Hill, The elastic behaviour of a crystalline aggregate, Proceedings of the Physical Society. Section A 65 (5) (1952) 349.

[6] H.-S. Shen, Nonlinear bending of functionally graded carbon nanotube-reinforced composite plates in thermal environments, Composite Structures 91 (1) (2009) 9–19.

[7] L. Zhang, K. Liew, J. Reddy, Postbuckling analysis of bi-axially compressed laminated nanocomposite plates using the first-order shear deformation theory, Composite Structures 152 (2016) 418–431.

[8] T. Mori, K. Tanaka, Average stress in matrix and average elastic energy of materials with misfitting inclusions, Acta metallurgica 21 (5) (1973) 571–574.

[9] L. Zhang, K. Liew, Geometrically nonlinear large deformation analysis of functionally graded carbon nanotube reinforced composite straight-sided quadrilateral plates, Computer Methods in Applied Mechanics and Engineering 295 (2015) 219–239.

[10] Z. Hashin, S. Shtrikman, A variational approach to the theory of the elastic behaviour of polycrystals, Journal of the Mechanics and Physics of Solids 10 (4) (1962) 343–352.

[11] T. O. Williams, A three-dimensional, higher-order, elasticity-based micromechanics model, International Journal of Solids and Structures 42 (3) (2005) 971–1007.

[12] M. Paley, J. Aboudi, Micromechanical analysis of composites by the generalized cells model, Mechanics of materials 14 (2) (1992) 127–139.

[13] E. J. Pineda, A. M. Waas, B. A. Bednarcyk, C. S. Collier, P. W. Yarrington, Progressive damage and failure modeling in notched laminated fiber reinforced composites, International journal of fracture 158 (2) (2009) 125–143.

[14] W. Drugan, J. Willis, A micromechanics-based nonlocal constitutive equation and estimates of representative volume element size for elastic composites, Journal of the Mechanics and Physics of Solids 44 (4) (1996) 497–524.

[15] T. Kanit, S. Forest, I. Galliet, V. Mounoury, D. Jeulin, Determination of the size of the representative volume element for random composites: statistical and numerical approach, International Journal of solids and structures 40 (13) (2003) 3647–3679.

[16] W. Yu, T. Tang, Variational asymptotic method for unit cell homogenization of periodically heterogeneous materials, International Journal of Solids and Structures 44 (11) (2007) 3738–3755.

[17] W. Yu, A unified theory for constitutive modeling of composites, Journal of Mechanics of Materials and Structures 11 (4) (2016) 379–411.

[18] X. Liu, W. Yu, A novel approach to analyze beam-like composite structures using mechanics of structure genome, Advances in Engineering Software 100 (2016) 238–251.

[19] A. De Miguel, A. Pagani, W. Yu, E. Carrera, Micromechanics of periodically heterogeneous materials using higher-order beam theories and the mechanics of structure genome, Composite Structures 180 (2017) 484–496.

[20] J. LLorca, C. González, J. M. Molina-Aldareguía, J. Segurado, R. Seltzer, F. Sket, M. Rodríguez, S. Sádaba, R. Muñoz, L. P. Canal, Multiscale modeling of composite materials: a roadmap towards virtual testing, Advanced Materials 23 (44) (2011) 5130–5147.

[21] T. M. Ricks, T. E. Lacy, E. J. Pineda, B. A. Bednarcyk, S. M. Arnold, Computationally efficient high-fidelity generalized method of cells micromechanics via order-reduction techniques, Composite Structures 156 (2016) 2–9.

[22] E. Carrera, Theories and finite elements for multilayered plates and shells: a unified compact formulation with numerical assessment and benchmarking, Archives of Computational Methods in Engineering 10 (3) (2003) 215–296.

[23] E. Carrera, S. Brischetto, Analysis of thickness locking in classical, refined and mixed theories for layered shells, Composite Structures 85 (1) (2008) 83–90.

[24] E. Zappino, G. Li, A. Pagani, E. Carrera, Global-local analysis of laminated plates by node-dependent kinematic finite elements with variable esl/lw capabilities, Composite Structures 172 (2017) 1–14.

[25] E. Carrera, G. Giunta, Refined beam theories based on a unified formulation, International Journal of Applied Mechanics 2 (01) (2010) 117–143.

[26] E. Carrera, G. Giunta, P. Nali, M. Petrolo, Refined beam elements with arbitrary cross-section geometries, Computers & Structures 88 (5) (2010) 283–293.

[27] E. Carrera, M. Petrolo, Refined one-dimensional formulations for laminated structure analysis, AIAA journal 50 (1) (2012) 176–189.

[28] M. Filippi, A. Pagani, M. Petrolo, G. Colonna, E. Carrera, Static and free vibration analysis of laminated beams by refined theory based on chebyshev polynomials, Composite Structures 132 (2015) 1248–1259.

[29] A. Pagani, A. De Miguel, M. Petrolo, E. Carrera, Analysis of laminated beams via unified formulation and legendre polynomial expansions, Composite Structures 156 (2016) 78–92.

[30] E. Carrera, M. Maiarú, M. Petrolo, Component-wise analysis of laminated anisotropic composites, International Journal of Solids and Structures 49 (13) (2012) 1839–1851.

[31] M. Maiarú, M. Petrolo, E. Carrera, Evaluation of energy and failure parameters in composite structures via a component-wise approach, Composites Part B: Engineering 108 (2017) 53–64.

[32] I. Kaleel, M. Petrolo, A. Waas, E. Carrera, Computationally efficient, high-fidelity micromechanics framework using refined 1d models, Composite Structures.

[33] M. Dan, A. Pagani, E. Carrera, Free vibration analysis of simply supported beams with solid and thin-walled cross-sections using higher-order theories based on displacement variables, Thin-Walled Structures 98 (2016) 478–495.

[34] Y. Yan, A. Pagani, E. Carrera, Exact solutions for free vibration analysis of laminated, box and sandwich beams by refined layer-wise theory, Composite Structures 175 (2017) 28–45.

[35] A. Pagani, Y. Yan, E. Carrera, Exact solutions for static analysis of laminated, box and sandwich beams by refined layer-wise theory, Composites Part B: Engineering.

[36] G. Giunta, F. Biscani, S. Belouettar, A. Ferreira, E. Carrera, Free vibration analysis of composite beams via refined theories, Composites Part B: Engineering 44 (1) (2013) 540–552.

[37] G. Giunta, S. Belouettar, H. Nasser, E. Kiefer-Kamal, T. Thielen, Hierarchical models for the static analysis of three-dimensional sandwich beam structures, Composite Structures 133 (2015) 1284–1301.

[38] E. Carrera, M. Maiarú, M. Petrolo, G. Giunta, A refined 1d element for the structural analysis of single and multiple fiber/matrix cells, Composite Structures 96 (2013) 455–468.

[39] E. Carrera, G. Giunta, M. Petrolo, Beam structures: classical and advanced theories, John Wiley & Sons, 2011.

[40] K.-J. Bathe, Finite element procedures, Klaus-Jurgen Bathe, 2006.

[41] E. Carrera, M. Cinefra, M. Petrolo, E. Zappino, Finite element analysis of structures through unified formulation, John Wiley & Sons, 2014.

[42] N. J. Pagano, Exact solutions for composite laminates in cylindrical bending, Journal of Composite Materials 3 (3) (1969) 398–411.

[43] M. Tahani, Analysis of laminated composite beams using layerwise displacement theories, Composite Structures 79 (4) (2007) 535–547.